

Lawrence Berkeley National Laboratory

Lawrence Berkeley National Laboratory

Title

Simple Model Representations of Transport in a Complex Fracture and Their Effects on Long-Term Predictions

Permalink

<https://escholarship.org/uc/item/5v00b07j>

Author

Tsang, Chin-Fu

Publication Date

2008-06-10

Peer reviewed

1
2

3 Simple Model Representations of Transport in a Complex Fracture and
4 Their Effects on Long-Term Predictions

5
6

7 Chin-Fu Tsang¹, Christine Doughty¹, and Masahiro Uchida²

8

9 ¹Earth Sciences Division, Lawrence Berkeley National Laboratory

10 Berkeley, California 94720, USA

11

12 ²Geological Isolation Research and Development Directorate, Japan Atomic Energy

13 Agency

14 Akeyo-cho, Mizunami-shi, Gifu, 509-6132, Japan

15

16

17 Revised April 2008

18

19 **Abstract**

20

21 A complex fracture model for fluid flow and tracer transport was previously developed
22 that incorporates many of the important physical effects of a realistic fracture, including
23 advection through a heterogeneous fracture plane, partitioning of flow into multiple
24 subfractures in the third dimension, and diffusion and sorption into fracture-filling gouge,

25 small altered rock matrix blocks within the fracture zone, and the unaltered semi-infinite
26 rock matrix on both sides of the fracture zone (Tsang and Doughty, 2003). It is common,
27 however, to represent the complex fracture by much simpler models consisting of a single
28 fracture, with a uniform or heterogeneous transmissivity distribution over its plane and
29 bounded on both sides by a homogeneous semi-infinite matrix. Simple-model properties
30 are often inferred from the analysis of short-term (one to a few days) site characterization
31 (SC) tracer-test data. The question addressed in this paper is: How reliable is the
32 temporal upscaling of these simplified models? Are they adequate for long-term
33 calculations that cover thousands of years? In this study, a particle-tracking approach is
34 used to calculate tracer-test breakthrough curves (BTCs) in a complex fracture model,
35 incorporating all the features described above, for both a short-term SC tracer test and a
36 10,000-year calculation. The results are considered the “real-world”. Next, two simple
37 fracture models, one uniform and the other heterogeneous, are introduced. Properties for
38 these simple models are taken either from laboratory data or found by calibration to the
39 short-term SC tracer-test BTCs obtained with the complex fracture model. Then the
40 simple models are used to simulate tracer transport at the long-term time scale. Results
41 show that for the short-term SC tracer test, the BTCs calculated using simple models with
42 laboratory-measured parameters differ significantly from the BTCs obtained with the
43 complex fracture model. By adjusting model properties, the simple models can be
44 calibrated to reproduce the peak arrival time and height of the complex-fracture-model
45 BTCs, but the overall match remains quite poor. Using simple models with short-term
46 SC-calibrated parameters for long-term calculations causes order-of-magnitude errors in
47 tracer BTCs: peak arrival time is 10–100 times too late, and peak height is 50-300 times

48 too small. On the other hand, using simple models with laboratory-measured properties of
49 unfractured rock samples for 10,000-year calculations results in peak arrivals and heights
50 up to a factor of 50 too early and large, respectively. The actual magnitudes of the errors
51 made by using the simple models depend on the parameter values assumed for the
52 complex fracture model, but in general, simple models are not expected to provide
53 reliable long-term predictions. The paper concludes with some suggestions on how to
54 improve long-term prediction calculations.

55

56

57 **1.0 Introduction**

58 Flow and transport in fractured rock are critical hydrological elements in many
59 important practical problems, such as subsurface contaminant migration and safety of a
60 nuclear waste geological repository. A review of this research area, with a discussion of
61 trends and challenges, was presented by Neuman (2005), who also provided a
62 comprehensive list of references. An earlier review by Tsang and Neretnieks (1998)
63 systematically presented important field experiments on tracer transport at different
64 spatial scales and some associated theoretical studies. During the past decade, a number
65 of major multiyear field and modeling investigations of transport in fractured rocks have
66 been reported. These include studies at the Mirror Lake site (Becker and Shapiro, 2003;
67 Shapiro, 2001; Shapiro and Hsieh, 1991), the so-called TRUE project at Äspö
68 (Andersson et al., 2004; Winberg et. al., 2003), and investigations of fractured dolomite
69 at Carlsbad (Meigs and Beauheim, 2001; Haggerty et al., 2001; McKenna et al., 2001).

70

71 Generally, these efforts involved field measurements of migration of tracers that were
72 introduced into a fracture or fracture system through an injection well. Data interpretation
73 and modeling studies are used to estimate key parameters associated with transport in a
74 fracture, such as fracture porosity or aperture and matrix diffusion coefficient. Guimerá
75 and Carrera (2000) made an interesting study of the parameters from a large number of
76 tracer tests and attempted to understand their dependence on spatial and temporal scales.
77 Zhou et al (2007) also conducted a survey of measured values of the effective matrix
78 diffusion coefficient for fractured rock at scales from meters to kilometers and showed a
79 scale dependence with larger values for increasing spatial scale.

80

81 The parameters thus evaluated can be used in models to predict migration of tracers in
82 fractured rocks. Using tracer migration data to determine parameters characteristic of a
83 site is part of the site characterization (SC) process, and prediction of tracer migration
84 tens to thousands of years into the future is part of what is known as “performance
85 assessment” (PA). A discussion of the key issues involved in going from SC to PA is
86 given in Tsang (2005) and also in Tsang et al. (1994). One of the issues is the
87 development of appropriate conceptual structural models for modeling transport through
88 fractured rock (Hodgkinson and Black, 2005; Reimus et al., 2003; Mazurek et al., 2003
89 and Jakob et al., 2003).

90

91 Most of the field and modeling studies to date consider a fracture to be uniform over
92 its plane (on scales of a meter to tens or even hundreds of meters), implying that it can be
93 characterized by its mean aperture value and a diffusion coefficient describing solute

94 diffusion into the surrounding rock matrix. A justification for this often-made
95 simplification is that detailed data on deviations from this simple conceptual picture of
96 the fracture are often not available or hard to come by. Nevertheless, there are definite
97 field data to show that fractures are not so simple (Mazurek et al., 2001; Robinson et al.,
98 1998; Bossart and Mazurek, 1991). The goal of the present paper is to study tracer
99 transport in a complex fracture (defined below) and evaluate the accuracy of long-term
100 predictions of tracer transport made by very much simplified conceptual models of the
101 fracture. Generally, features of tracer transport that have important PA implications are
102 the first tracer arrival time, the peak concentration, and persistence of the concentration
103 tail. However, in this paper we do not focus on these PA issues, but rather discuss the
104 more basic question of how well are the tracer breakthrough curves (BTC) predicted in
105 term of their effective porosity, which controls tracer arrival time, and their effective
106 matrix diffusion coefficient, which controls the peak concentration. These two
107 parameters, porosity and diffusion coefficient, are also the usual ones used in analysis of
108 tracer breakthrough curves from field tests (e.g., Chilès and deMarsily, 1993; Cvetkovic
109 et al., 2007; Widestrand et al., 2007).

110

111 Based on geological observations presented in Mazurek et al. (2001), a complex
112 fracture model for fluid flow and tracer transport was previously developed that
113 incorporates many of the important physical effects of a complex fracture layer, including
114 advection through a heterogeneous fracture plane, partitioning of flow into multiple
115 subfractures in the third dimension, and diffusion and sorption into fracture-filling gouge,
116 small altered rock matrix blocks within the fracture zone, and the unaltered semi-infinite

117 rock matrix on both sides of the fracture zone (Tsang and Doughty, 2003). Generally, the
118 model takes its initial values for material properties from laboratory data and then
119 modifies them by calibration to short-term SC data, such as breakthrough curves for
120 tracer migration tests lasting one to a few days. We shall refer to these tests with duration
121 of a few days as short-term site characterization or “stSC” data. The model can then be
122 used for PA calculations, which track tracer migration for thousands of years, typically
123 under much lower hydraulic gradients than are imposed during SC tracer tests. Note that
124 SC tracer tests with duration of weeks or months are also feasible, but in the present
125 study we assume that only short-term tests of one day’s duration have been conducted.

126

127 As mentioned above, it is common to represent the complex fracture, which is
128 considered to be the “real world” in this paper, by much simpler models consisting of a
129 single fracture, which may have a uniform or heterogeneous transmissivity distribution
130 over its plane and is bounded on both sides by a homogeneous semi-infinite matrix. The
131 parameters of the simple model can be evaluated by calibration to stSC data or by
132 laboratory measurements on core samples of rock in the vicinity of the fracture. The
133 question posed by this paper is, how adequate are these simplified models for long-term
134 PA calculations? It will be shown below that the stSC and PA results, corresponding to
135 different time frames, are sensitive to different parts of the parameter set of the “real-
136 world” complex fracture, and thus care needs to be exercised in the use of parameter
137 values obtained from calibration with stSC tests, and perhaps much longer tests than the
138 one-day SC test will be needed.

139

140 The paper is organized as follows. First, we present an overview of the conceptual
141 model for the complex fracture and describe the numerical model used for the flow and
142 transport calculations. Then, sensitivity studies of tracer breakthrough curves (BTCs) to
143 various model parameters over a range of values are discussed. Next, two simple fracture
144 models are introduced to represent the complex fracture model, one with a single
145 heterogeneous fracture (without subfractures or internal materials) and the other with a
146 uniform fracture of constant aperture. Finally, we proceed to investigate potential errors
147 that the simple models may introduce into their long-term PA predictions. Some remarks
148 on how to improve long-term predictions conclude the paper.

149

150

151 **2.0 Complex Fracture Model**

152 This section presents a brief overview of the complex fracture model developed by
153 Tsang and Doughty (2003), where details of the model may be found. Figure 1 shows the
154 complex fracture model, in which advection occurs in a two-dimensional (2D)
155 heterogeneous fracture plane with a transmissivity distribution given by $T(x,y)$, from
156 which flow $q(x,y)$ can be calculated given the hydraulic pressure imposed on boundaries..
157 Fracture structure in the third (z) dimension is accounted for by dividing flow $q(x,y)$
158 among multiple subfractures. In this figure, two sub-fractures are shown, for which

159

$$160 \quad q = q_1 + q_2 \quad (1)$$

161

162 The partitioning of flow between subfractures is controlled by the fracture structure
163 parameter α , by defining

164

$$165 \quad q_2 = \alpha q_1 \quad (2)$$

166

167 The value of α can range from 0 (only a single subfracture) to 1 (two identical
168 subfractures). The entire fracture plane is characterized by a single α value.

169

170 Diffusion and sorption occur into three materials surrounding the fracture:

- 171 • Fault gouge within the fractures (conceptualized as small blocks of rock)
- 172 • Altered rock within the fracture zone (intermediate-size blocks of rock)
- 173 • Unaltered rock outside the fracture zone (a semi-infinite rock matrix)

174

175 The parameter controlling matrix diffusion is the effective diffusion coefficient D_e , given
176 by $D_e = D_{fw}\phi_m\tau$, where D_{fw} is free-water diffusion coefficient, ϕ_m is matrix porosity, and
177 τ is matrix tortuosity ($\tau \leq 1$, with $\tau = 1$ indicating a direct, nontortuous path and smaller
178 values of τ corresponding to more tortuous paths). The sorption coefficient is K_d . Each of
179 the three materials has its own values of K_d , ϕ_m and τ (and therefore D_e), and a
180 characteristic length scale denoted $2r_m$.

181

182 A customized version of the numerical model THEMM (Tsang and Tsang, 2001) is
183 used to calculate flow and transport. First, a heterogeneous 2D fracture transmissivity
184 distribution $T(x,y)$ is created, using program SISIM from GSLIB (Deutsch and Journel,

185 1998). The T field has a stochastic heterogeneity in which the correlation length can be
186 made to depend on the T level. In our case, a larger value is used for the higher 20% of T
187 values to represent the well-known consideration that larger transmissivity tends to be
188 associated with a larger spatial correlation length. In general, SISIM allows anisotropic T
189 fields, but the one created here is isotropic.

190

191 Local fracture aperture $w(x,y)$ is assumed to be related to local $T(x,y)$ according to
192 the cubic law

193

$$194 \quad T(x,y) = w^3(x,y) / [12(\mu/\rho g)] , \quad (3)$$

195

196 where μ is viscosity, ρ is fluid density, and g is acceleration due to gravity. Then, local
197 fracture porosity $\phi_f(x,y)$ is obtained from $w(x,y)$ according to

198

$$199 \quad \phi_f(x,y) = 3w(x,y)/\Delta z. \quad (4)$$

200

201 where Δz is the thickness of the complex fracture zone, typically a few centimeters and
202 assumed constant over the fracture plane, and the factor of three accounts for the fact that
203 fractures may be oriented in any of the three spatial dimensions within the fracture zone.

204 Mean fracture porosity ϕ_f is then defined as the porosity value obtained from Equations
205 (3) and (4) using the geometric mean of $T(x,y)$ in Equation (3) rather than $T(x,y)$ itself.

206 This derivation for $\phi_f(x,y)$ differs from the original version of THEMME, in which fracture

207 porosity was taken to be a constant over the entire fracture plane, equal to the mean value
208 ϕ_f .

209

210 Table 1 summarizes the model dimensions and heterogeneous fracture properties used for
211 the present paper, which are representative of a real fracture zone at the Äspö
212 Underground Research Laboratory in Sweden (Doughty and Uchida, 2003).

213

214 The flow field $q(x,y)$ is calculated by a finite-difference method, then tracer transport
215 is calculated using particle tracking. When a particle arrives at a grid block, first an
216 advective residence time t_w is calculated based on the 2D flow field. For the i^{th} grid block
217 at location (x,y) , denote $q(x,y) = q_i$ and $\phi_f(x,y) = \phi_{fi}$:

218

$$219 \quad t_w = \frac{\phi_{fi} \Delta x \Delta y \Delta z}{\frac{1}{2} \sum_{j=1}^J |q_{ij}|} \quad (5)$$

220 where q_{ij} is the flow between the i^{th} grid block and each of its J neighbors. Each particle
221 is introduced into one of the two subfractures in the third dimension, which is chosen
222 randomly, weighted by the α parameter. As the particle moves in this sub-fracture, the
223 residence time is modified by assuming that a local cubic law holds in the subfractures
224 (Tsang and Doughty, 2003).

225

226 Next, one of the three rock matrix materials is chosen at random, according to pre-
227 assigned likelihoods based on the proportion of each material present, and a residence-
228 time increment (delay) is calculated to represent diffusion and sorption into the material,

229 by inverting an analytical solution (Rasmuson and Neretnieks, 1981). In the analytical
230 solution, the finite volumes of the fault gouge and altered rock within the fracture zone
231 are accounted for, which limits their capacity for diffusion and sorption. As these finite
232 materials become saturated, the corresponding residence-time increment decreases to
233 zero. For a given grid block, if the residence-time increment for gouge or altered rock is
234 less than the increment that would be obtained for the semi-infinite matrix (unaltered
235 rock outside the fracture zone), then the semi-infinite-matrix-based increment is applied
236 instead. This algorithm corresponds to a conceptualization in which saturated gouge and
237 altered rock do not shield the fluid particles from interacting with the semi-infinite
238 matrix. In previous studies (Tsang and Doughty, 2003), we used a different
239 conceptualization, in which fluid particles encountering saturated gouge or altered rock
240 did not have a chance to interact with the semi-infinite matrix. It turns out that for SC
241 time scales, tracer BTCs produced by the two prescriptions only differ in their late-time
242 tails, with identical peak arrival times and heights. In contrast, for PA time scales, the two
243 prescriptions produce BTCs that differ from each other. The present prescription has the
244 advantage that when the gouge and intermediate blocks are saturated, the BTCs tend to
245 the simple case of diffusion into the bounding semi-infinite rock matrix.

246

247 For the present studies we consider two different tracers, tritiated water (HTO), which
248 is nonsorbing, and Sr, which is slightly sorbing. Table 2 summarizes the properties of the
249 three rock matrix materials, which were obtained from laboratory measurements and by
250 calibrating the complex fracture model to a tracer test conducted using two boreholes
251 packed off in the fracture zone at Äspö, Sweden (Doughty and Uchida, 2003). Note that

252 the parameters for effective diffusion and sorption are much higher for gouge material
253 and intermediate blocks than the semi-infinite rock matrix because they have undergone
254 much larger mechanical and chemical disturbances than the intact rock corresponding to
255 the semi-infinite matrix.

256

257 Tracer transport is calculated for a pulse tracer release in a steady-state flow field. For
258 SC, the flow field represents a radially converging tracer test with tracer traveling about 5
259 m and breakthrough observed over a few days. Pumping rate, test duration, and well
260 separation are based on the parameters of an actual tracer experiment conducted at Äspö
261 Hard Rock Laboratory (Doughty and Uchida, 2003). For PA, a natural hydraulic gradient
262 creates a linear flow field. Tracer is released over a 2 m wide zone and collected over a
263 15 m wide zone, 10 m downgradient from the release location. Tracer arrivals occur over
264 thousands of years. Table 3 summarizes the characteristics of the two flow fields. Note
265 that hydraulic gradient is several orders of magnitude larger for the SC flow field than for
266 the PA flow field, to enable the SC tracer test to be conducted within a reasonable time
267 frame. Figure 2 illustrates the heterogeneous T field and the PA flow field. The T field is
268 moderately heterogeneous, causing localized channels of preferential flow to develop
269 (Moreno and Tsang, 1994; Tsang and Tsang, 1989).

270

271

272 **3.0 Sensitivity of Tracer Breakthrough Curves to Features of Complex Fracture**

273 **Model**

274 The key output of the complex fracture model is the tracer breakthrough curve (BTC),
275 that is, the tracer concentration C as a function of time at a specified location, which is
276 represented by a single well for SC and the downgradient boundary of the fracture model
277 for PA. For a pulse tracer release, the key characteristics of the tracer BTC (Chilès and
278 deMarsily, 1993) may be defined as:

- 279 • Peak arrival time t_{pk}
- 280 • Peak height C_{pk}
- 281 • Peak shape - quantified by the first arrival time t_1 (which we take as the time at
282 which $C \approx 10^{-3}C_{pk}$) and the rate of decrease in the tail region

283 Figure 3 illustrates stSC tracer BTCs for the complex model with parameters given in
284 Tables 1-2, with the three points t_{pk} , C_{pk} , and t_1 marked. In the subsections below, we
285 examine the impact of various features of the complex fracture model on these BTC
286 characteristics.

287

288 ***3.1 Fracture Heterogeneity***

289 To explore the effect of heterogeneity over the fracture plane on tracer BTCs, we
290 conducted a series of short-term site characterization (stSC) simulations omitting matrix
291 diffusion and sorption. Thus, tracer transport occurs purely by advection through the
292 fracture. Moreover, we consider only one subfracture by taking $\alpha = 0$. The top frame of
293 Figure 4 shows the resulting tracer BTCs for T fields with four levels of heterogeneity
294 (created by increasing $\sigma_{\log T}$ in the heterogeneous field generator, SISIM, while keeping
295 all other parameters unchanged). As $\sigma_{\log T}$ increases, the peak height decreases, the peak
296 becomes broader, and the peak arrival time is delayed. The lowering of peak height and

297 broadening of peak width occur as more diverse flow paths are encountered within the
298 more variable T fields. The peak arrival is delayed because fluid flows preferentially into
299 localized high transmissivity regions, which have high fracture porosity and consequently
300 a longer advective residence time. The bottom frame of Figure 4 shows the corresponding
301 tracer BTCs obtained with the full complex fracture model, with two subfractures and
302 three materials for matrix diffusion and sorption. All peaks are later, lower, and broader
303 due to the addition of matrix diffusion, and they show a small second peak arising from
304 flow through the smaller of the two subfractures. However, the effect of increasing
305 fracture heterogeneity is unchanged.

306

307 Work elsewhere (Moreno and Tsang, 1994) has shown that for even larger values of
308 $\sigma_{\log T}$ (e.g., 3), earlier and sharper peaks may develop as flow becomes so focused that
309 large portions of the fracture network are bypassed. This is the strong channeling case. In
310 such a case, the early peak is accompanied by a long late-time tail which includes effects
311 of diffusion not only into rock matrix, but also into “stagnant” water region between
312 channels in the fracture plane. The value of $\sigma_{\log T} = 1.35$ (Table 1) used in the current
313 study has not reached this regime.

314 **3.2 Mean Fracture Porosity ϕ_f**

315 The mean fracture porosity ϕ_f controls the peak arrival time, with arrival time longer
316 as ϕ_f increases. The peak height also decreases with increasing ϕ_f , as the slower travel
317 time allows more matrix diffusion and sorption to occur. Figure 5 shows stSC tracer
318 BTCs for five values of ϕ_f . Note that ϕ_f is the fraction of void space within the complex
319 fracture zone, not within the fractured rock block as a whole. In this sensitivity

320 calculation, we have varied ϕ_f without changing T, which is not internally consistent, but
321 this is often done in calibration exercises, in which measured T values are used in tracer
322 transport modeling and ϕ_f is independently varied to match the BTCs (see, e.g., Chilès
323 and deMarsily, 1993; Cvetkovic et al., 2007; Widestrand et al., 2007)
324

325 ***3.3 Fracture Structure Parameter α***

326 Fracture structure parameter α , corresponding to the ratio of flows through the two
327 subfractures, can range from 0 to 1. Figure 6 shows stSC tracer BTCs for ten α values
328 within this range. For $\alpha = 0$, there is only one subfracture, and for $\alpha = 1$, there are two
329 identical subfractures, so in both of these two cases the shape of the BTCs is controlled
330 by fracture heterogeneity (compare Figure 4). For the smallest non-zero α value (0.01),
331 the fraction of flow occurring through the smaller subfracture, $q_2 = \alpha q_1$, is so small that it
332 does not affect the BTC noticeably. For $\alpha = 0.03$, the peak arrival time and height are
333 unchanged, but a second, much smaller and much later peak is present, reflecting flow
334 through the smaller subfracture. For $\alpha \geq 0.1$, flow through the smaller subfracture is
335 significant enough to delay the arrival and decrease the height of the main peak (less flow
336 through the larger subfracture). For $\alpha \geq 0.5$, no individual second peak is visible, but an
337 extended tail of the main peak shows the contribution of flow through the smaller
338 subfracture. For $\alpha = 1$, the two identical subfractures provide greater fracture porosity
339 than a single subfracture ($\alpha = 0$) does. This ϕ_f dependence on α can be explained by
340 considering that the two subfractures each obey the cubic law (Equation 3), and that the
341 sum of their flows or transmissivities is fixed (Equation 1). This means that $(w_1^3 + w_2^3) =$

342 $w_1^3(1+\alpha) = \text{constant}$, so that porosity (Equation 4), being proportional to $(w_1 + w_2) =$
343 $w_1(1+\alpha^{1/3})$, becomes a function of α . From this it can be shown directly that the $\alpha=1$ case
344 has a larger porosity and thus would have a later, lower peak. Note that for small α
345 values, if monitoring does not continue long enough or measurement sensitivity is not
346 high enough, the second peak may not be observed. Then the only observable effect of
347 increasing α will be to delay arrival time and decrease the height of the peak, much like
348 the effect of increasing ϕ_f .

349

350 *3.4 Matrix Diffusion and Sorption*

351 The time-scale on which matrix diffusion and sorption occur depends strongly on the
352 diffusion properties of the rock blocks, with the gouge having the fastest diffusion and
353 strongest sorption (until it is saturated), and the semi-infinite matrix having the slowest
354 diffusion and weakest sorption. Figure 7 shows tracer BTCs for stSC tracer tests with a
355 nonsorbing tracer for the full complex fracture model, with diffusion into three matrix
356 materials, and for two variations: one with diffusion occurring only into the gouge
357 material and the other with diffusion occurring into the gouge and intermediate-size
358 matrix blocks within the fracture zone, but not into the semi-infinite matrix outside the
359 fracture zone. For all cases, $\alpha=0.03$.

360

361 It is apparent that for tracer tests lasting a few days, the calculated BTC is essentially
362 insensitive to diffusion into the semi-infinite rock matrix; it is nearly two days before the
363 full complex fracture model BTC differs appreciably from the BTCs for the cases with no
364 diffusion into semi-infinite rock. Moreover, for the period including the tracer peak, the

365 BTC is primarily controlled by diffusion into the gouge. Hence, a stSC tracer test
366 provides the most information on gouge properties, some limited information on
367 intermediate-size matrix blocks, and little if any information on the semi-infinite rock
368 matrix properties. Longer tests would be required for the intermediate-size matrix blocks
369 and the semi-infinite matrix to have a noticeable effect on stSC tracer BTC.

370

371

372 **4.0 Simple Fracture Models and an Approach to Study the Relationship between** 373 **SC-calibrated, Laboratory-measured and PA Transport Parameters**

374 The previous two sections present the complex fracture model and how the
375 breakthrough curves (BTCs) of tracer transport through it depend on its parameters. In
376 practical field studies of flow and transport through fractures, such detailed parameters of
377 a complex fracture are normally not available. Often a single fracture (i.e., no
378 subfractures) with a constant aperture (constant transmissivity) over its plane is used to
379 represent the complex fracture. The focus of this and following sections is to study
380 whether such a simplified representation of the complex fracture (which is taken as the
381 “real world”) can adequately reproduce flow and transport, and what errors are
382 introduced into long-term prediction of tracer BTCs by such a simplification.

383

384 Instead of one simple fracture model, we shall consider two models, both of which
385 account for advection through a planar fracture and diffusion and sorption into a
386 homogeneous semi-infinite rock matrix. In one case, the fracture has a uniform
387 transmissivity T over its plane, and in the other case, it has the same heterogeneous

388 $T(x,y)$ field as in the complex fracture model. Here it is assumed that the $T(x,y)$ for the
389 heterogeneous model is known. Then the geometric mean transmissivity $\langle T \rangle$ is used as
390 the transmissivity for the simple uniform model. Once $\langle T \rangle$ and $T(x,y)$ are defined, the
391 only parameters in either of the two simple models are ϕ_f and D_e . The features present in
392 the complex fracture model that are absent from both the simple models are the
393 partitioning of flow between multiple subfractures, and diffusion and sorption into gouge
394 and finite blocks of altered rock within the fracture zone. These will be accounted for
395 approximately through the use of “effective values” of ϕ_f and D_e .

396

397 We use the complex fracture model to produce tracer BTCs for both stSC and PA
398 time scales and conditions, which are the synthetic “real world” results. We then apply
399 the two simple fracture models to stSC and PA problems and compare the resulting tracer
400 BTCs to those of the complex fracture model, adjusting the simple model parameter
401 values of ϕ_f and D_e to optimize the match. There are three sets of effective values of ϕ_f
402 and D_e that will be used in the discussions below:

- 403 • $\phi_{f(SC)}$ and $D_{e(SC)}$, values resulting from calibration against stSC data, which are
404 from tracer tests of short durations of a few days.
- 405 • $\phi_{f(PA)}$ and $D_{e(PA)}$, values resulting from fitting against PA results of the complex
406 model (the ‘real world’). This is of course not something that can be obtained in
407 field cases. Here they are calculated and used for comparison with other effective
408 values to study errors made in extrapolation to long-term predictions.
- 409 • $\phi_{f(Lab)}$ and $D_{e(Lab)}$, values obtained by laboratory measurements on rock samples
410 from the two sides of the complex fracture. These laboratory-determined

411 parameter values correspond to the semi-infinite rock matrix values used in the
412 complex fracture model.

413

414

415 **5.0 Results**

416 **5.1 SC Calibration**

417 Figure 8 shows the tracer BTCs for nonsorbing HTO and slightly-sorbing Sr, under
418 stSC conditions (a converging radial tracer test) for the complex fracture model,
419 considering two different values of fracture structure parameter α , with the upper frame
420 of the figure showing the case of $\alpha=0$ and the lower frame showing $\alpha=0.6$. Also
421 presented in the figure are the BTCs obtained from a simple heterogeneous fracture
422 model using (a) the $D_{e(Lab)}$ and $\phi_{f(Lab)}$ values and (b) the calibrated $D_{e(SC)}$ and $\phi_{f(SC)}$
423 values. For reference, a tracer BTC for an advection-only model (heterogeneous fracture,
424 $\alpha = 0$, no rock matrix) is also plotted. Because the different diffusion and sorption
425 coefficients of HTO and Sr only affect interactions with the rock matrix, the advection-
426 only models for HTO and Sr yield identical BTCs. The simple models with laboratory
427 parameters also yield nearly indistinguishable BTCs for HTO and Sr. This is expected,
428 considering that the parameter groups controlling matrix diffusion, $D_e\phi_m$ for non-sorbing
429 HTO and $D_eK_d\rho_p$ for slightly-sorbing Sr, happen to be nearly the same (see Table 2).

430

431 The complex fracture model BTC is significantly different from the advection-only
432 BTC, with a later, lower, broader peak. In contrast, the heterogeneous simple fracture
433 model BTCs for the original values of D_e and ϕ_f (i.e., $D_{e(Lab)}$ and $\phi_{f(Lab)}$) differ from the

434 advection-only BTC only at late times, showing a longer tail. This implies that in our
435 case for the SC time scale, the features present only in the complex fracture model—flow
436 through multiple subfractures and diffusion and sorption into gouge and intermediate-size
437 matrix blocks—have a significant impact, whereas diffusion and sorption into the semi-
438 infinite matrix have a minor effect. By increasing D_e and ϕ_f (see Table 4), the simple
439 model can match the timing, height, and width of the peak of the complex model BTCs,
440 although the details of the tails of the BTCs are not well matched. Increasing α from 0 to
441 0.6 results in somewhat lower and later peaks, requiring larger values of $D_{e(SC)}$ and $\phi_{f(SC)}$.
442 Note that in this discussion, a comparison is made between the complex fracture model
443 and the calibrated simple models. In practice, increased D_e and ϕ_f can be due to other
444 physical effects such as micro-fractures on both sides of the fracture plane.

445

446 Figure 9 shows the analogous results to Figure 8 for the uniform simple fracture
447 model. The advection-only BTC for a uniform fracture is much narrower than that for the
448 heterogeneous fracture. The uncalibrated simple model BTCs (obtained with $D_{e(Lab)}$ and
449 $\phi_{f(Lab)}$) differ from the advection-only BTC only at late times, confirming that diffusion
450 and sorption into the semi-infinite matrix are too slow to affect peak timing or height. By
451 increasing D_e and ϕ_f (see Table 4), the calibrated simple model BTCs can match the peak
452 arrival time and height of the complex model BTCs, but the peaks remain too narrow, a
453 consequence of the lack of heterogeneity in the fracture plane.

454

455 Table 4 summarizes the parameter values required to match the stSC tracer BTCs
456 shown in Figure 8 and Figure 9. D_e must be increased by a factor of 100–700 for the

457 heterogeneous simple model and by a factor of 3,000–12,000 for the uniform simple
458 model, and ϕ_f must be increased by a factor of 4–12 for the heterogeneous simple model
459 and by a factor of 13–34 for the uniform simple model. These increases delay, broaden,
460 and lower the height of the peak, thus mimicking the features of the complex model that
461 are missing from the simple models: principally the enhanced diffusion and sorption that
462 occur in the fault gouge and altered rock matrix within the complex fracture zone. The
463 larger increases required for the uniform simple model reflect the additional broadening
464 process, fracture heterogeneity, which is missing from the uniform simple model.

465

466 The left-hand column of Figure 10 summarizes the results of the SC calibration of the
467 heterogeneous and uniform simple models for a range of α values. Increasing α results in
468 greater pore space for fluid flow, thus requiring increases in $\phi_{f(SC)}$. Intermediate values of
469 α provide the best opportunity for flow along disparate pathways, with the most
470 significant spreading of tracer arrival times, and these cases therefore require the largest
471 values of $D_{e(SC)}$.

472

473 **5.2 PA Calibration**

474 Figure 11 shows the tracer BTCs for nonsorbing HTO and slightly-sorbing Sr, under
475 PA conditions (long-term and linear flow under a regional head gradient) for the complex
476 fracture model, considering two values of α , and the BTCs for a heterogeneous simple
477 fracture model. For the simple model, BTCs obtained using the original values $D_{e(Lab)}$
478 and $\phi_{f(Lab)}$, and calibrated values $D_{e(SC)}$, $\phi_{f(SC)}$, $D_{e(PA)}$, and $\phi_{f(PA)}$ are all shown. Also
479 plotted is a tracer BTC for an advection-only model (heterogeneous fracture, $\alpha = 0$, no

480 rock matrix), for which HTO and Sr yield identical BTCs. The complex fracture model
481 shows a later, lower, broader peak than does the advection-only model, along with a
482 much longer tail, indicating that matrix diffusion and sorption are important processes at
483 PA time scales. With the laboratory parameters, the simple model produces a peak arrival
484 time that is 3–10 times too early and a peak height that is 2–10 times too high, indicating
485 that fracture porosity, matrix diffusion, and sorption are being underestimated. When
486 using the stSC-calibrated parameters, the simple model produces a peak arrival time that
487 is 10–20 times too late and a peak height that is 50–100 times too small, indicating that
488 fracture porosity, matrix diffusion, and sorption are being greatly overestimated. By
489 calibration to the PA tracer curves, a good match to the peak arrival time, height, width,
490 and tail can be obtained for the heterogeneous simple fracture model.

491

492 Figure 12 shows the analogous results to Figure 11 for the uniform simple fracture
493 model. The general features of the original, stSC-calibrated, and PA-calibrated simple
494 models are similar to those shown in Figure 11 for a heterogeneous simple model: with
495 the laboratory parameters, peak arrival time is 10–30 times too early and peak height is
496 10–50 times too high. With the stSC-calibrated parameters, peak arrival time is about 100
497 times too late and peak height is 100–300 times too small. Moreover, the shape of the
498 BTC for the PA-calibrated uniform simple model does not match the complex model
499 result as well as did the heterogeneous simple model, producing too narrow a peak,
500 indicating that the effect of fracture heterogeneity cannot be correctly reproduced merely
501 by using effective values of fracture porosity, matrix diffusion, and sorption.

502

503 Table 4 summarizes the parameter values required to match the PA tracer BTCs
504 shown in Figure 11 and Figure 12. D_e must be increased by a factor of 2–9 for the
505 heterogeneous simple model and by a factor of 12–48 for the uniform simple model; ϕ_f
506 must be increased by a factor of 5–13 for the heterogeneous simple model and by a factor
507 of 9–20 for the uniform simple model. The center column of Figure 10 summarizes the
508 results of the PA calibration of the heterogeneous and uniform simple models for a range
509 of α values. The α dependence is very similar to that for stSC, with $\phi_{f(SC)}/\phi_{f(Lab)}$ steadily
510 increasing with increasing α , and $D_e(SC)/D_e(Lab)$ showing a modest maximum for
511 intermediate values of α .

512
513 As described above, the serious errors made when using a simple model with SC-
514 calibrated parameters for a PA simulation (Figures 11 and 12) arise because stSC time-
515 scale processes are dominated by fracture gouge properties, whereas PA-time-scale
516 processes are dominated by semi-infinite matrix properties. The results shown in Figures
517 11 and 12 employ a population fraction that is 25% gouge and 25% intermediate-size
518 matrix blocks. It is worthwhile to see if errors become negligible when the fractions of
519 fracture gouge and intermediate-size matrix blocks are much smaller. Complex fracture
520 models with $\alpha = 0$ and $\alpha = 0.6$, each with population fractions 10% gouge and 10%
521 intermediate-size matrix blocks, were used to simulate stSC and PA time-scale tracer
522 tests. Uniform and heterogeneous simple models were calibrated to the stSC tracer tests,
523 and the resulting values of $\phi_{f(SC)}$ and $D_{e(SC)}$ were used to simulate the PA time-scale
524 tracer test. Results (not shown) indicate that the errors made when simulating PA with
525 SC-calibrated properties for the are 10% gouge, 10% intermediate case are comparable to

526 errors obtained for the 25% gouge, 25% intermediate case. Considering that the diffusion
527 and sorption properties of the fault gouge and unaltered rock differ by up to three orders
528 of magnitude (Table 2), it is perhaps not surprising that merely decreasing the percent of
529 gouge from 25% to 10% has only a minor effect. The lesson is that even fracture systems
530 with small percentages of gouge and altered rock can exhibit very different behavior than
531 do simple systems with only unaltered rock matrix surrounding the fractures.

532

533 *5.3 Comparison of PA-calibrated transport parameters, SC-calibrated, and Laboratory-* 534 *measured parameters*

535 In Table 4, calibrated parameters are compared with laboratory-measured parameters.
536 The table entries show the parameter changes required to mimic the processes of the
537 complex fracture model that are missing in the simple models. In the complex model,
538 both the non-zero α and large gouge diffusion delay peak arrival; this is accomplished in
539 the simple models by modest increases in ϕ_f , which lengthen advective residence time. In
540 the complex model, the presence of gouge material enhances matrix diffusion, delaying,
541 lowering, and broadening the tracer peak; this is mimicked in the simple models with
542 large increases in D_e . Fracture heterogeneity has a similar effect on the tracer peak, so
543 even larger increases in D_e are required for the uniform simple model.

544

545 In Table 5 and the right-hand column of Figure 10, SC-calibrated parameters are
546 compared with PA-calibrated parameters. Note that if the flow and transport processes
547 did not have a strong time dependence—that is, if SC and PA processes were essentially
548 the same—then all the entries in Table 5 would be one. The $\phi_{f(SC)}/\phi_{f(PA)}$ ratios do not, in

549 fact, differ significantly from one, which is consistent with the notion that ϕ_f primarily
550 controls advective residence time, a quantity that does not have a strong time
551 dependence. In contrast, the $D_{e(SC)}/D_{e(PA)}$ ratios are much greater than one, because
552 matrix diffusion is dominated by gouge diffusion at SC time scales and by semi-infinite
553 matrix diffusion at PA time scales.

554

555

556 **6.0 Discussions and Conclusions**

557 We have examined the possibility of using simple fracture models, consisting of a
558 planar fracture, which may have a uniform transmissivity or a heterogeneous
559 transmissivity distribution, and which is bounded on either side by a homogeneous semi-
560 infinite rock matrix, to represent a complex fracture model (the “real world”). The latter
561 includes a heterogeneous transmissivity distribution, as well as multiple subfractures, and
562 diffusion and sorption into fracture-filling gouge and intermediate-size, altered rock
563 matrix blocks, and the semi-infinite rock matrix on either side of the fracture. The study
564 is based on comparing the effective parameters required for the simple models to
565 reproduce PA results at 10,000 years and SC results from stSC tracer tests as calculated
566 by the complex model (considered “the real world”). We find that by adjusting fracture
567 porosity ϕ_f and semi-infinite matrix diffusion coefficient D_e , simple fracture models can
568 reproduce the key features of an SC tracer test: peak height and timing are well matched,
569 while the BTC tail misses some detail. For a simple model with a uniform fracture
570 transmissivity distribution, the leading edge of the BTC is too sharp. PA tracer arrivals
571 can be matched comparably well, but the required effective D_e values differ by up to two

572 orders of magnitude from those obtained by stSC calibration with tracer duration of a few
573 days. Using stSC-calibrated parameters for PA calculations with the simple models
574 causes order-of-magnitude errors in tracer BTCs: peak arrival time is 10–100 times too
575 late and peak height is 50–300 times too small.

576

577 On the other hand, using laboratory-measured parameters of rock samples from
578 unfractured rock for PA calculations also produces erroneous results: peak arrivals and
579 heights can be up to a factor of 50 too early and high, respectively. These conclusions are
580 strongly dependent on the material properties of the fracture gouge, intermediate blocks,
581 and the semi-infinite medium used in the complex model. For example, they can be
582 opposite to what are stated if the matrix diffusion-sorption properties of the intermediate
583 blocks are weaker than those of the semi-infinite rocks on either side of the complex
584 fracture.

585

586 Thus, we conclude that simple models do not provide a reliable means of making PA
587 predictions, if stSC data are all that are available for calibration. Significant, though
588 smaller, errors are also introduced if laboratory-measured values are used. We suggest
589 that using a more realistic complex fracture model to interpret SC tracer test data could
590 enhance confidence of PA prediction and also allow temporal upscaling, especially when
591 tracer tests of a longer term than a few days are conducted. Further studies are under way
592 to evaluate the additional information that could be extracted from tracer tests of longer
593 durations. Preliminary calculations considering tracer tests of weeks to months' duration
594 show that, for our set of parameters, the gouge material and intermediate blocks gradually

595 become saturated with tracers for longer tests, so that the BTCs display more and more
596 the effects of the semi-infinite matrix. We are optimistic that by a combination of short
597 and long-term tracer tests we may be able to evaluate the appropriate parameter values
598 for long-term prediction of tracer transport. It should also be noted that using the complex
599 model directly as a basis for SC data analysis (even with a shortage of data and non-
600 uniqueness of parameters) has certain advantages, because it allows us to evaluate effects
601 of gouge materials in the fracture that are often observed in the field and to provide a way
602 to estimate uncertainties involved in long-term tracer transport calculations.

603

604 The present paper represents a first step in studying relationships between parameters
605 from laboratory experiments or from short-term tracer transport experiments and long-
606 term prediction of tracer transport for thousands of years, for the particular case of a
607 complex fracture. The actual real world involves features not in our complex fracture
608 model, such as micro-fractures on both sides of the fracture plane and flow across
609 multiple fractures in a network. Our study indicates the danger of presumptuously
610 modeling fractures or fault zones as simple fractures with homogeneous properties. There
611 is a need to have some information, even at a rough level, on the complexity of fractures
612 and fracture zones. Then such information can be used to improve prediction calculations
613 and also, by sensitivity analysis, to estimate the uncertainty ranges of the predictions,
614 which are a very important part of any long-term predictions.

615

616

617 **Acknowledgments**

618 We thank Kenzi Karasaki of Berkeley Lab and the anonymous WRR reviewers for
619 their careful review of this paper and most helpful comments. This work was supported
620 by the Japan Atomic Energy Agency (JAEA) under the Binational Research Cooperative
621 Program between JAEA and the Director, Office of Civilian Radioactive Waste
622 Management, of the U.S. Department of Energy under Contract No. DE-AC02-
623 05CH11231.

624

625

626 **References**

627 Andersson, P, J. Byegård, E.-L. Tullborg, T. Doe, J. Hermanson, and A. Winberg, In situ
628 tracer tests to determine retention properties of a block scale fracture network in granitic
629 rock at the Äspö Hard Rock Laboratory, Sweden. *J Cont Hydrology*, 70, pp 271-297,
630 2004.

631

632 Becker, M.W., and A.M. Shapiro, Interpreting tracer breakthrough tailing from different
633 forced-gradient tracer experiment configurations in fractured bedrock. *Water Resour Res*,
634 39(1), 1024, DOI: 10.1029/2001WR00190, 2003.

635

636 Bossart, P. and M. Mazurek, Grimsel Test Site-structural geology and water flow-paths in
637 the migration shear-zone. *NAGRA Tech Rep NTB 91-12*, Nagra, Wettingen, Switzerland,
638 1991.

639

640 Brown, S.R., A. Caprihan, and R. Hardy, Experimental observation of fluid flow
641 channels in a single fracture *J Geophys Res*, 103(B3), 5125–5132, 1998.
642

643 Chilès, J.-P. and G. deMarsily, Stochastic models of fracture systems and their use in
644 flow and transport modeling. Book Chapter in *Flow and Contaminant Transport in*
645 *Fractured Rocks*, edited by J. Bear, G. deMarsily and C. F. Tsang, Academic Press, pp.
646 169-236, 1993.

647

648 Cvetkovic, V., H. Cheng, H. Widestrand, J. Byegård, A. Winberg, and P. Andersson,
649 Sorbing tracer experiments in a crystalline rock fracture at Äspö (Sweden): 2. Transport
650 modeling and effective parameter estimation, *Water Resour Res*, 43, W11421,
651 doi:10.1029/2006WR005278, 2007.

652

653 Doughty, C. and M. Uchida, PA calculations for feature A with third-dimension structure
654 based on tracer test calibration, *Rep. IPR-04-33*, Swedish Nuclear Fuel and Waste
655 Management Co. (SKB), Stockholm, 2003.

656

657 Deutsch, C.V. and A.G. Journel, *GSLIB: Geostatistical software library and user's*
658 *guide*, 2nd ed., Oxford Univ. Press, New York 1998. Mazurek et al., 2001.

659

660 Guimerá, J., and J. Carrera, A comparison of hydraulic and transport parameters
661 measured in low-permeability fractured media, *J Cont Hydrology*, 41, 261–281, 2000.
662

663 Haggerty, R.R., S.W. Fleming, L.C. Meigs, and S.A. McKenna, Tracer tests in a
664 fractured dolomite, 2. Analysis of mass transfer in single-well injection-withdrawal tests.
665 *Water Resour Res* 37(5) 1129–1142, 2001.

666

667 Hodgkinson, D., and J. Black, Äspö Task Force on modelling of groundwater flow and
668 transport of solutes: Review of Tasks 6A, 6B, and 6B2, *SKB Tech Rep TR-05-14*, Svensk
669 Karnbranslehantering AB (SKB) Swedish Nuclear Fuel and Waste Management Co,
670 2005.

671

672 Jakob, A, M. Mazurek, and W. Heer, Solute transport in crystalline rocks at Äspö II:
673 Blind predictions, inverse modelling and lessons learnt from test STTI. *J Cont*
674 *Hydrology*, 61, 175-190, 2003.

675

676 Mazurek, M., P. Bossart, and J. Hermanson, Classification and characterization of water-
677 conducting features at Äspö, in *Proceedings of International Seminar First TRUE Stage*
678 *Rep. TR-01-24*, pp. 203-208, Swedish Nuclear Fuel and Waste Management Co. (SKB),
679 Stockholm, 2001.

680

681 Mazurek, M, A. Jakob, and P. Bossart, Solute transport in crystalline rocks at Äspö -I:
682 Geological basis and model calibration. *J Cont Hydrology*, 61, 157-174, 2003.

683

684 McKenna, S.A., L.C. Meigs, and R.R. Haggerty, Tracer tests in a fractured dolomite, 3.
685 Double porosity, multiple-rate mass transfer processes in convergent flow tracer tests.
686 *Water Resour Res*, 37(5) 1143–1154, 2001.
687
688 Meigs, L.C., and R.L. Beauheim, Tracer tests in fractured dolomite, 1. Experimental
689 design and observed tracer recoveries, *Water Resour Res*, 37(5) 1113–1128, 2001.
690
691 Moreno, L., and C. F. Tsang, Flow channeling in strongly heterogeneous porous media:
692 A numerical study, *Water Resour Res*, 30 (5), 1421–1430, 1994.
693
694 Neuman, S.P., Trends, prospects, and challenges in quantifying flow and transport
695 through fractured rocks, *Hydrogeol Jour*, 13, 124–147, 2005.
696
697 Rasmuson, A. and I. Neretnieks, Migration of radionuclides in fissured rock: The
698 influence of micropore diffusion and longitudinal dispersion, *J. Geophys Res*, 86(B5),
699 3749–3758, 1981.
700
701 Reimus, P, G. Pohll, T. Mihevc, J. Chapman, M. Raga, B. Lyles, S. Kosinski, R.
702 Niswonger, and P. Sanders, Testing and parameterizing a conceptual model for solute
703 transport in a fractured granite using multiple tracers in a forced gradient test. *Water*
704 *Resour Res* 39(12), 1356, DOI: 10.1029/ 2002WRR001597, 2003.
705

706 Robinson, N., J.M. Sharp, Jr., and I. Kreisel, Contaminant transport in sets of parallel
707 finite fractures with fracture skins. *J Cont Hydrology*, 31, 83–109, 1998.
708

709 Shapiro, A.M., Effective matrix diffusion in kilometer-scale transport in fractured
710 crystalline rock. *Water Resour Res*, 37(3), 507–522, 2001.
711

712 Tsang, C.-F. Is Current Hydrogeologic Research Addressing Long-Term Predictions?
713 *Ground Water*, 43 (3), 296–300. 2005.
714

715 Tsang, C.-F. and C. Doughty, A particle-tracking approach to simulating transport in a
716 complex fracture, *Water Resour Res*, 39(7), 1174, doi:10.1029/2002WR001614, 2003.
717

718 Tsang, C.-F., L. Gelhar, G. de Marsily, and J. Andersson, Solute transport in
719 heterogeneous media: A discussion of technical issues coupling site characterization and
720 predictive assessment. *Adv in Water Resour*, 17 (4), 259–264, 1994.
721

722 Tsang, C.-F. and I. Neretnieks, Flow channeling in heterogeneous fractured rocks. *Rev*
723 *Geophys*, 36(2), 275–298, 1998.
724

725 Tsang, Y.W. and C.-F. Tsang, Flow channeling in a single fracture as a two-dimensional
726 strongly heterogeneous permeable medium, *Water Resour Res*, 25 (9), 2076–2080, 1989.
727

728 Tsang, Y.W. and C.-F. Tsang, A particle-tracking method for advective transport in
729 fractures with diffusion into finite matrix blocks, *Water Resour Res*, 37(3), 831–835,
730 2001.

731

732 Widestrand, H., J. Byegård, V. Cvetkovic, E.-L. Tullborg, A. Winberg, P. Andersson, and
733 M. Siitari-Kauppi, Sorbing tracer experiments in a crystalline rock fracture at Äspö
734 (Sweden): 1. Experimental results and micro-scale characterization of retention
735 properties, *Water Resour Res*, 43, W10413, doi:10.1029/2006WR005277, 2007.

736

737 Winberg, A, P. Andersson, A. Poteri, V. Cvetkovic, W. Dershowitz, J. Hermanson, J.J.
738 Gomez-Hernandez, A. Hautjarvi, D. Billaux, E.-L. Tullborg, D. Holton, P. Meier, and
739 A. Medina, Final report of the TRUE Block Scale project, 4. Synthesis of flow, transport
740 and retention in the block scale. *SKB Technical Report TR-02-16*, Swedish Nuclear Fuel
741 and Waste Management Co., Stockholm, Sweden, 2003.

742

743 Zhou, Q., H.H. Liu, F.J. Molz, Y. Zhang, and G.S. Bodvarsson, Field scale effective
744 matrix diffusion coefficient for fractured rock: Results from literature survey. *J Cont*
745 *Hydrology*, 93, 161-187, 2007.

746 **Tables**

747

748 Table 1. Model dimensions and heterogeneous fracture properties for a reference case

749 that is representative of a real fracture (Doughty and Uchida, 2003).

Parameter	Value
Fracture dimensions (m)	15, 15, 0.02
nx, ny, nz (number of grid blocks)	150, 150, 1
$\Delta x, \Delta y, \Delta z$ (m) (grid spacing)	0.10, 0.10, 0.02
Sequential indicator simulation using a CDF for $\log_{10}T$ based on 15 well-test analyses for 5 boreholes	
Mean, standard deviation $\log_{10}T$ (T in m^2/s)	-6.5, 1.35
Spherical variogram range – for lower 80% of T values	0.3 m
Spherical variogram range – for higher 20 % of T values	1 m
Mean fracture porosity ϕ_f	0.011
Fracture structure parameter α	0.03

750 Table 2. Properties of three rock matrix materials for a reference case that is
 751 representative of a real fracture (Doughty and Uchida, 2003).

	Small blocks (fault gouge)	Intermediate blocks (altered rock inside ladder structure)	Semi-infinite matrix (unaltered rock outside ladder structure)
Proportion	0.25	0.25	0.5
Radius r_m (m)	$5 \cdot 10^{-4}$	0.005	not applicable (essentially infinite)
Porosity ϕ_m	0.2	0.01	0.004
Tortuosity τ	0.625	0.0625	0.0125
Density ρ_p (kg/m^3)	2700	2700	2700
D_{fw} (m^2/s)	HTO: $2.35 \cdot 10^{-9}$ Sr: $7.90 \cdot 10^{-10}$		
Effective Diffusion Coefficient D_e (m^2/s)	HTO: $2.9 \cdot 10^{-10}$ Sr: $9.9 \cdot 10^{-11}$	HTO: $1.5 \cdot 10^{-12}$ Sr: $4.9 \cdot 10^{-13}$	HTO: $1.2 \cdot 10^{-13}$ Sr: $4.0 \cdot 10^{-14}$
Sorption coefficient K_d (m^3/kg)	HTO: 0 Sr: $1.5 \cdot 10^{-4}$	HTO: 0 Sr: $4.7 \cdot 10^{-6}$	HTO: 0 Sr: $4.7 \cdot 10^{-6}$

752 Table 3. Comparison of flow fields for SC and PA.

	Site Characterization (SC):	Performance Assessment (PA):
	Two-well tracer test	Natural gradient
Flow field	Radial converging ($Q = 0.4$ L/min, hydraulic gradient approximately 1 m/m)	Linear (hydraulic gradient 0.001 m/m)
Tracer injection period	10 minutes	1 day
Particle release location	One well	2 m wide zone
Particle collection location	One well, 5 m away from release location	15 m wide zone (width of fracture), 10 m down-gradient from release location
Time of tracer observation	Main peak; 1-2 days Tail: up to 2 months	Peak: 1-5 years Tail: up to 2,000 years

753 Table 4. Summary of parameter values required in Figures 8–12 for simple models to
 754 match SC and PA tracer BTCs produced by the complex fracture model.

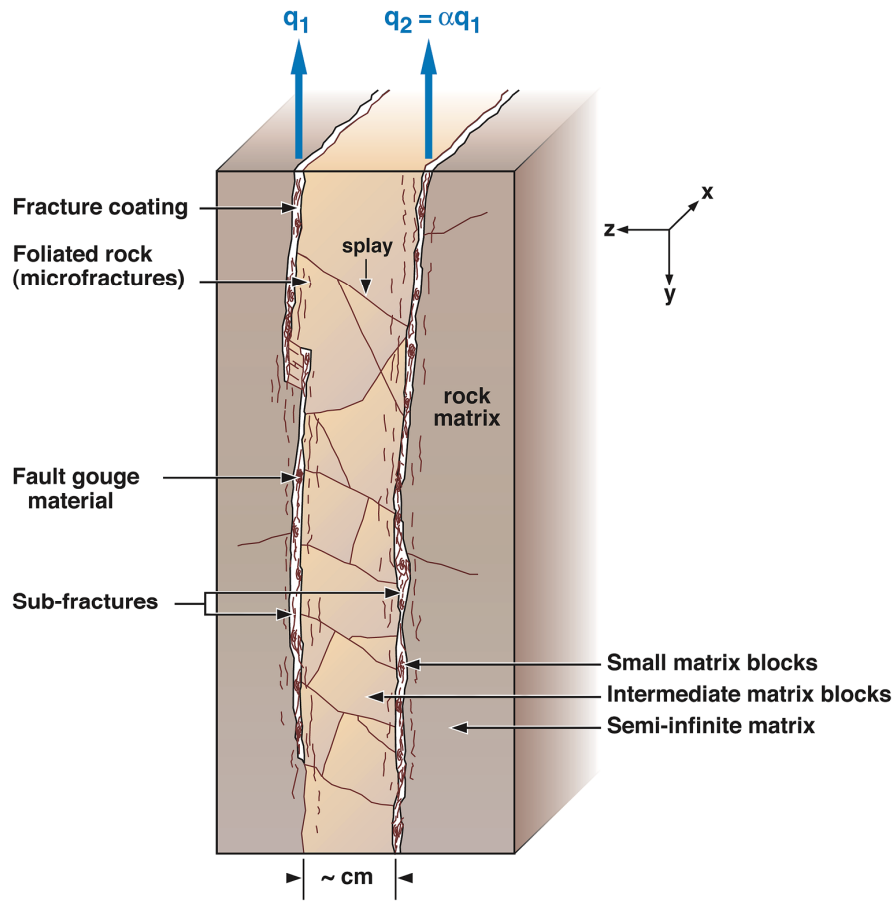
		SC		PA	
		Heterogeneous	Uniform	Heterogeneous	Uniform
$\alpha = 0$		$\phi_f(\text{SC})/\phi_f(\text{Lab})$		$\phi_f(\text{PA})/\phi_f(\text{Lab})$	
	HTO	4.5	13	5.3	9.0
	Sr	8.0	23	9.5	17
		$D_e(\text{SC})/D_e(\text{Lab})$		$D_e(\text{PA})/D_e(\text{Lab})$	
	HTO	120	2,800	1.8	12
	Sr	236	4,724	2.0	13
$\alpha = 0.6$		$\phi_f(\text{SC})/\phi_f(\text{Lab})$		$\phi_f(\text{PA})/\phi_f(\text{Lab})$	
	HTO	7.0	19	7.4	9.5
	Sr	12	34	13	20
		$D_e(\text{SC})/D_e(\text{Lab})$		$D_e(\text{PA})/D_e(\text{Lab})$	
	HTO	400	6,800	7.6	42
	Sr	709	11,811	8.8	48

755 Table 5. Comparison of SC-calibrated parameters with PA-calibrated parameters. The
 756 ratios shown are for $\alpha = 0$, but the right-hand column of Figure 10 shows that the ratios
 757 are not very sensitive to α .

Two simple models		Heterogeneous	Uniform
Fracture porosity factor $\phi_{f(SC)} / \phi_{f(PA)}$	HTO	0.85	1.44
	Sr	0.84	1.35
Diffusion factor (semi-infinite rock) $D_{e(SC)} / D_{e(PA)}$	HTO	65	233
	Sr	118	369

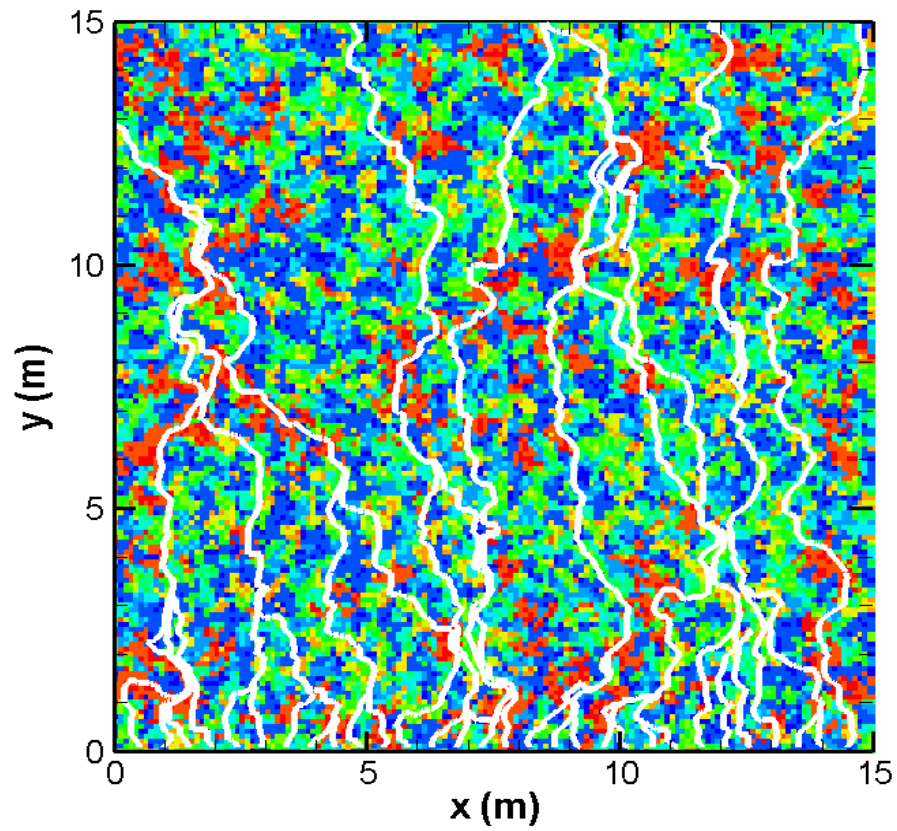
758 **Figures**

759



760

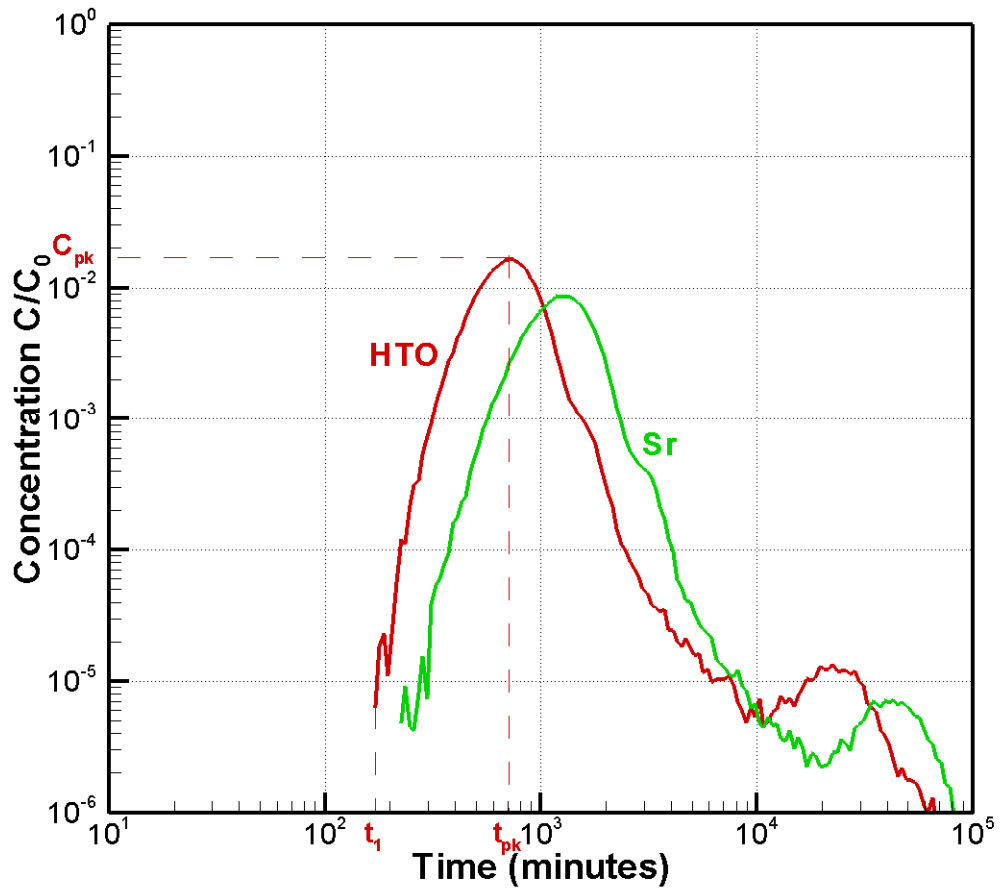
761 Figure 1. Schematic diagram of the complex fracture model (after Mazurek et al., 2001).



762

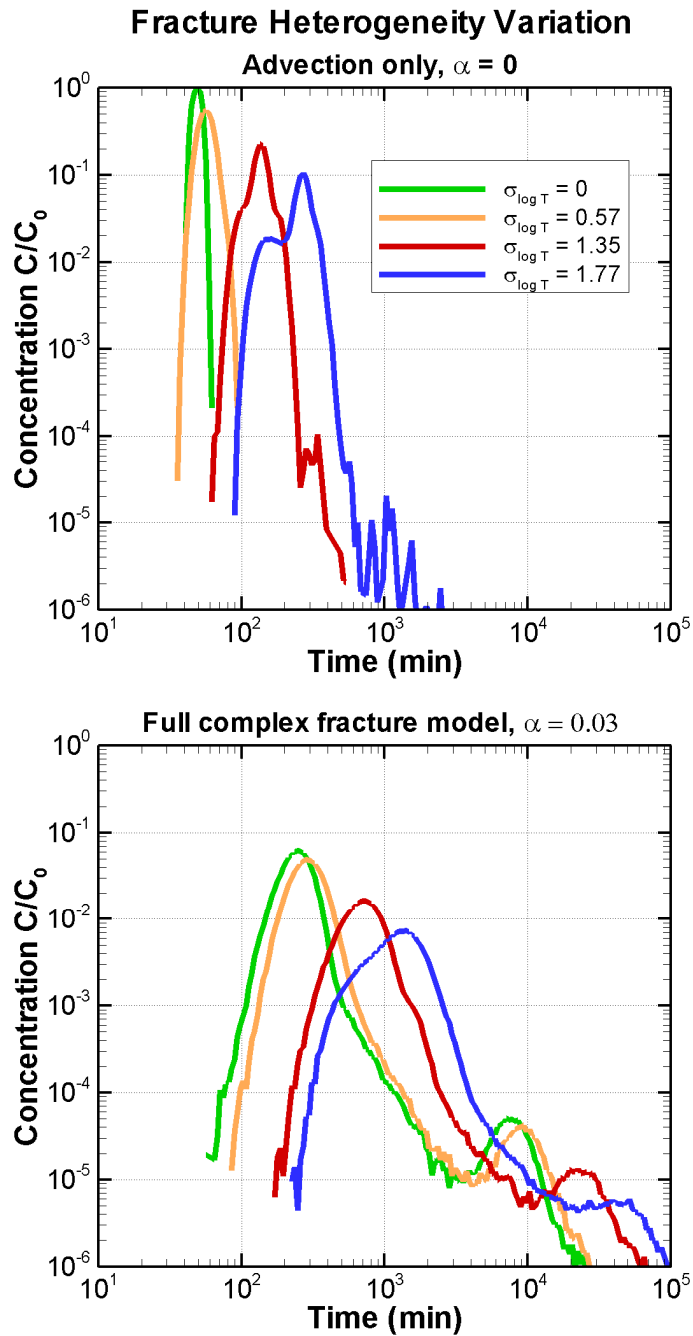
763 Figure 2. Fracture transmissivity field $T(x,y)$ for $\sigma_{\log T} = 1.35$: red is high T , blue is low

764 T ; flow lines show PA flow field, with flow from bottom to top.



765

766 Figure 3. Site-characterization (SC) tracer breakthrough curves (BTCs) calculated with
 767 the complex model, illustrating the three characteristics used to compare BTCs for
 768 different models: first arrival time t_1 , peak arrival time t_{pk} , and peak height C_{pk} .



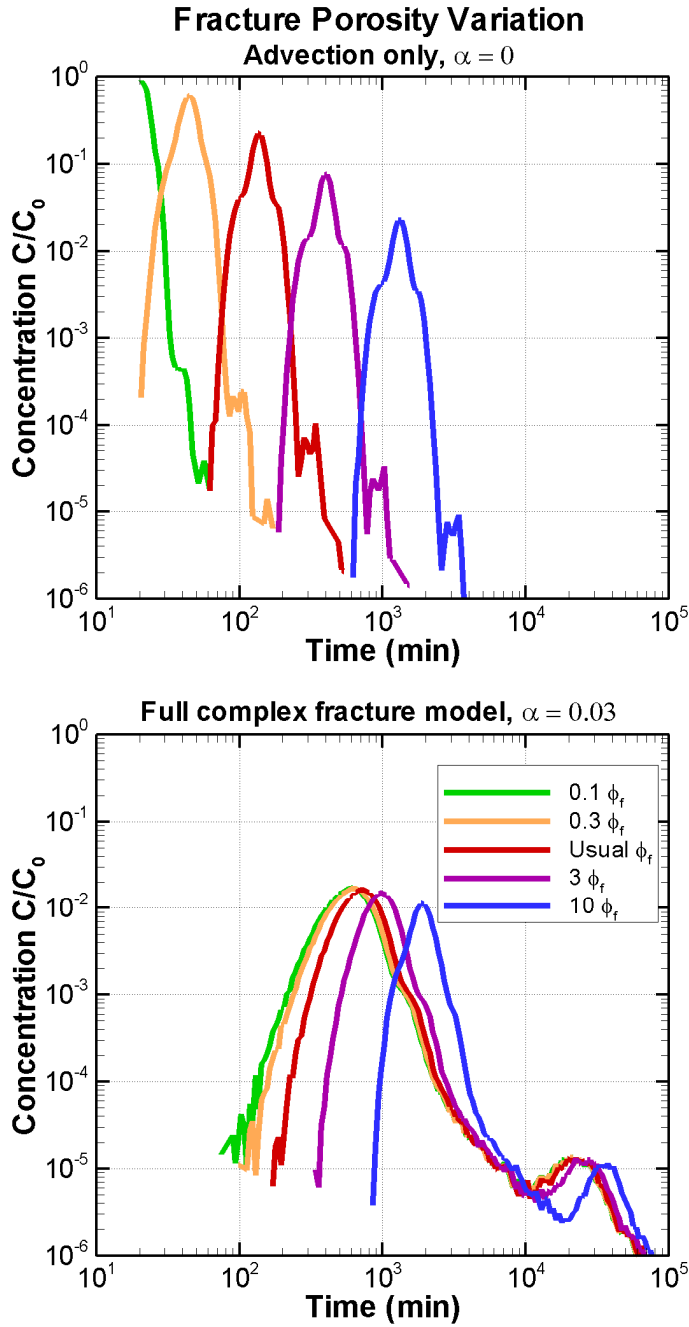
769

770 Figure 4. SC tracer BTCs for cases with different amounts of fracture heterogeneity. Top

771 frame: advection-only (no matrix diffusion or sorption) and only one subfracture ($\alpha = 0$);

772 bottom frame: full complex fracture model with $\alpha = 0.03$, and 25% gouge, 25%

773 intermediate blocks, and 50% semi-infinite matrix.



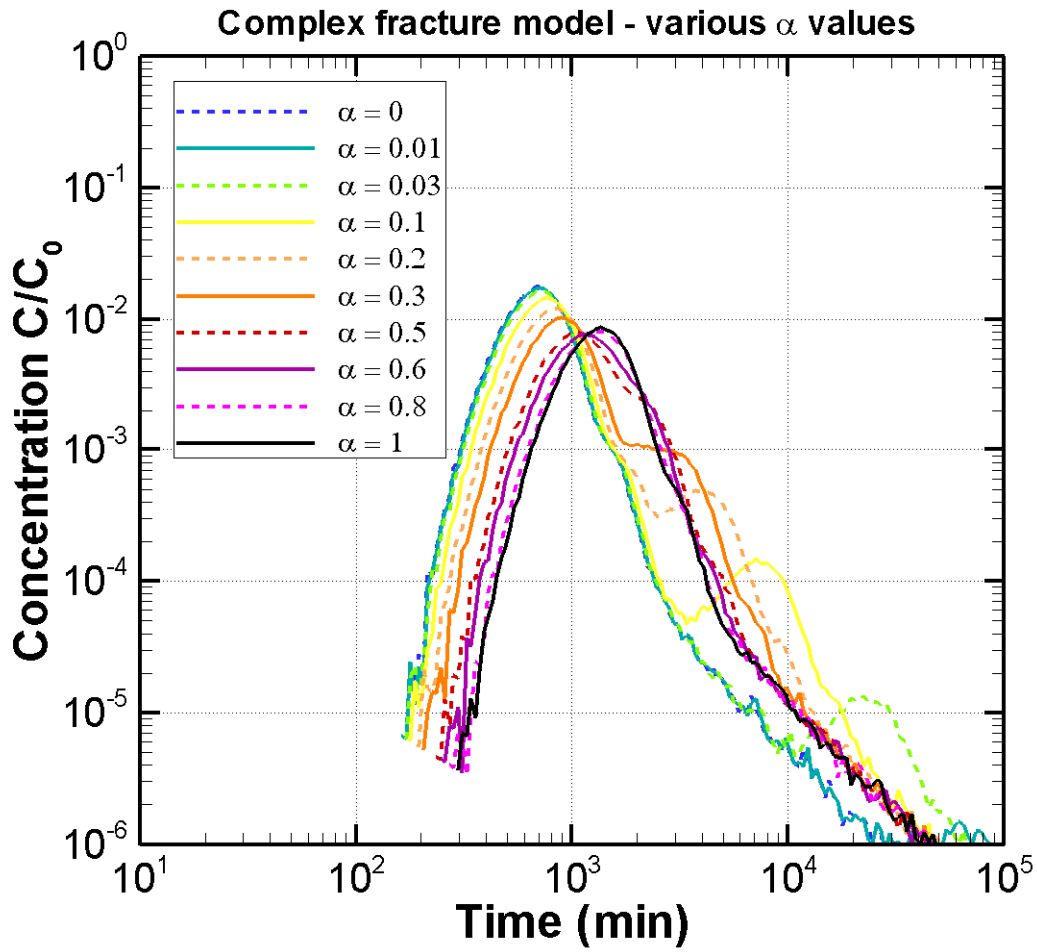
774

775 Figure 5. SC tracer BTCs for cases with different values of mean fracture porosity ϕ_f . Top

776 frame: advection-only (no matrix diffusion or sorption) and only one subfracture ($\alpha = 0$);

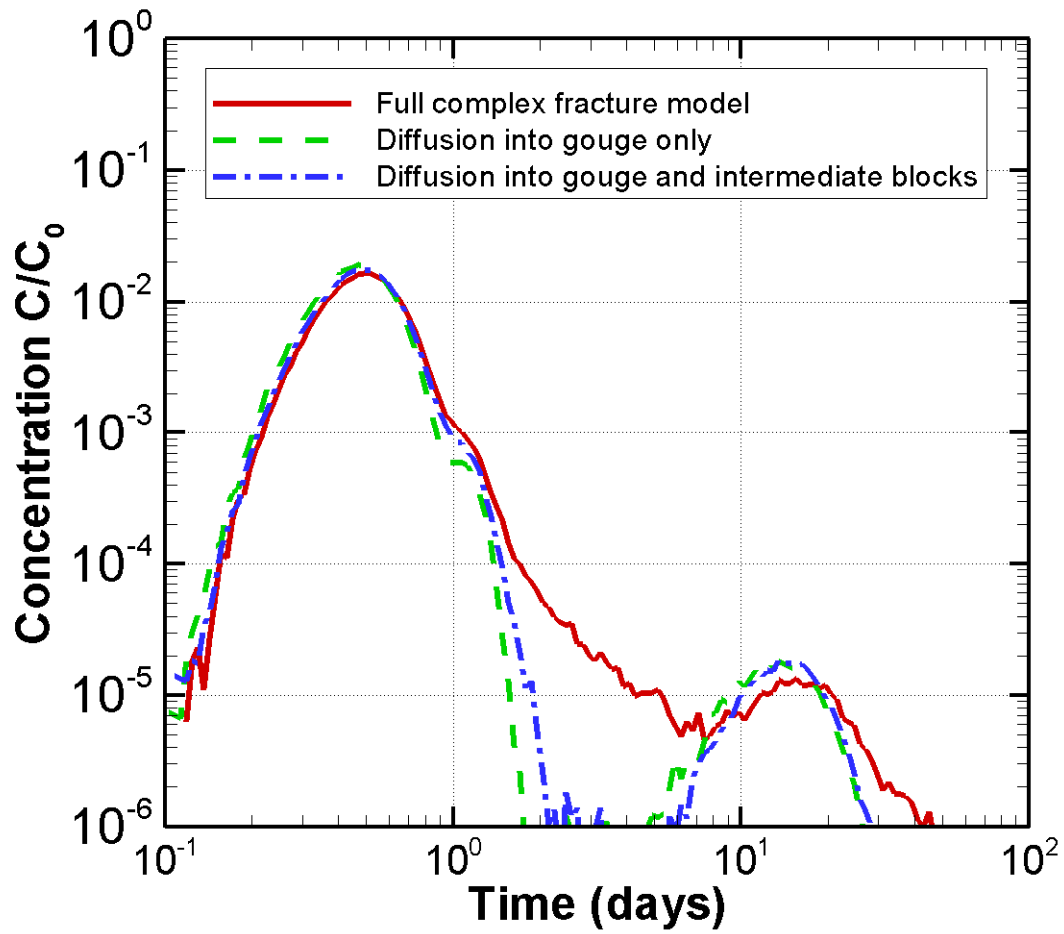
777 bottom frame: full complex fracture model with $\alpha = 0.03$, and 25% gouge, 25%

778 intermediate blocks, and 50% semi-infinite matrix.



780

781 Figure 6. SC tracer BTCs for various values of fracture structure parameter α .

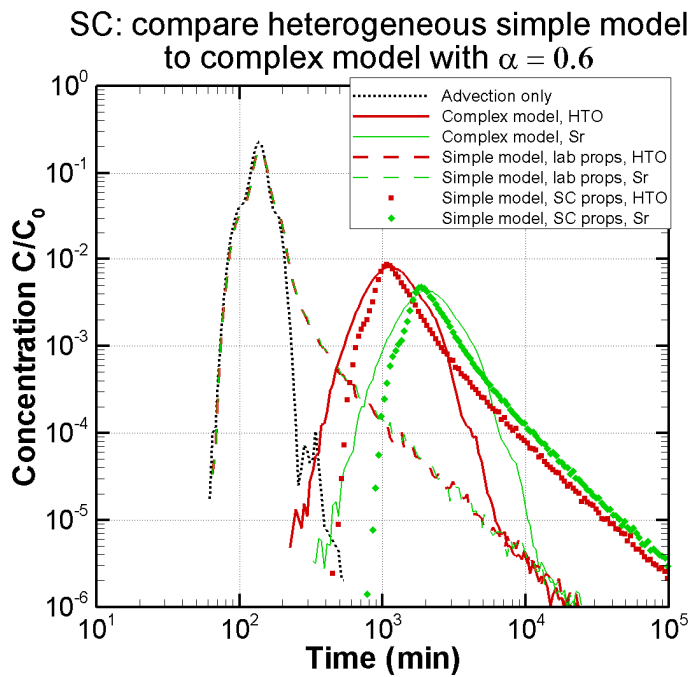
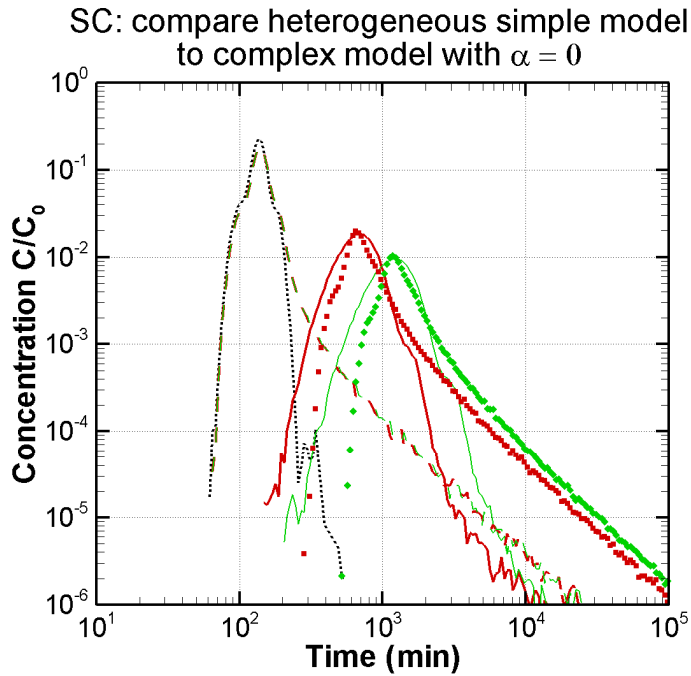


782

783 Figure 7. SC tracer BTCs with diffusion into various materials turned off. Divergence

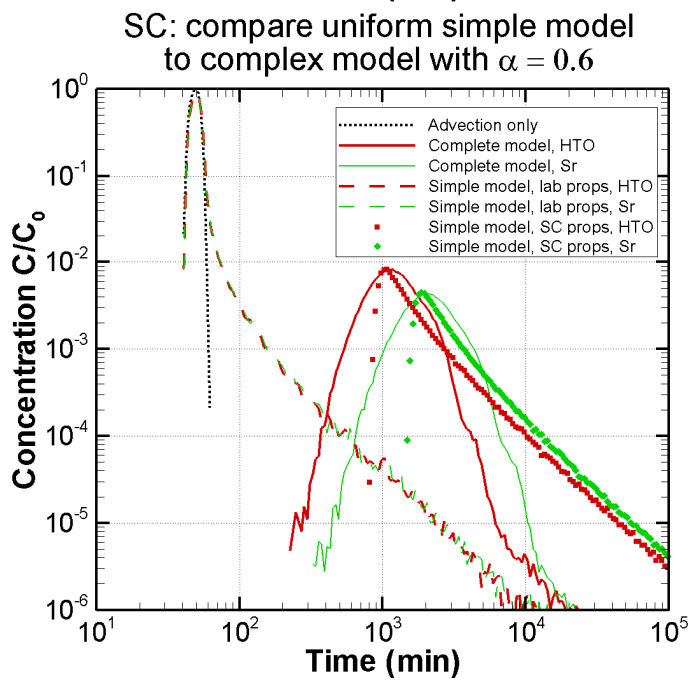
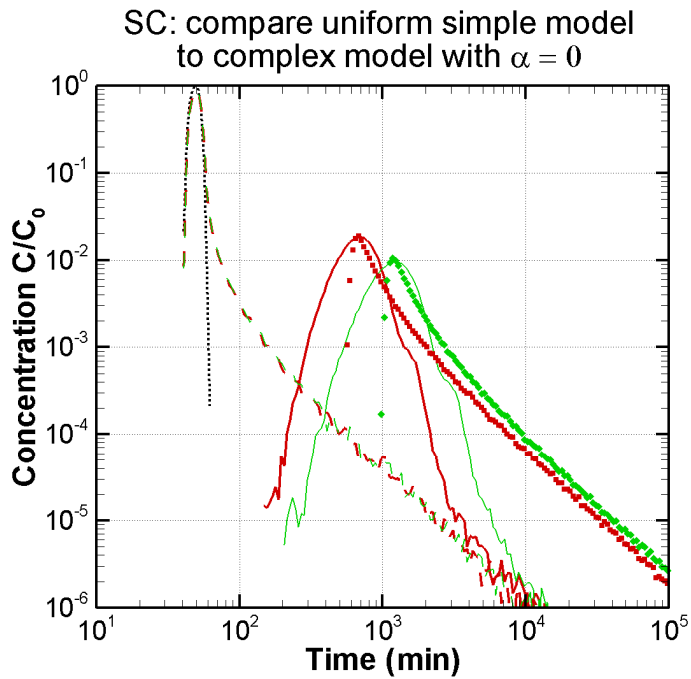
784 between the different curves illustrates when the effect of diffusion into different rock

785 matrix materials becomes apparent.



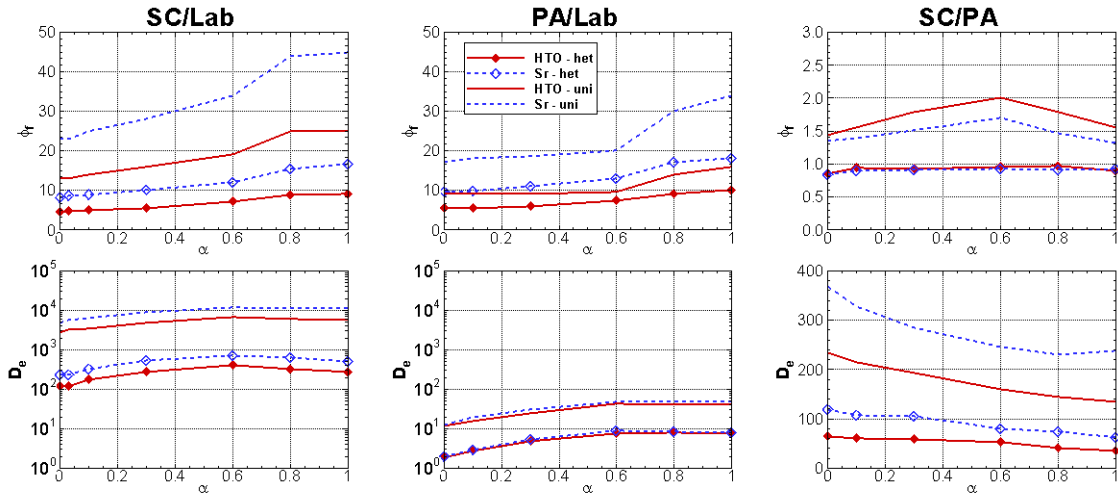
786

787 Figure 8. SC tracer BTCs for the complex fracture model and two versions of the
 788 heterogeneous simple fracture model (the original model with laboratory-measured
 789 properties and the model calibrated to SC), for two values of fracture structure parameter
 790 α . Results for advection-only through a heterogeneous fracture with $\alpha = 0$ are also
 791 shown.



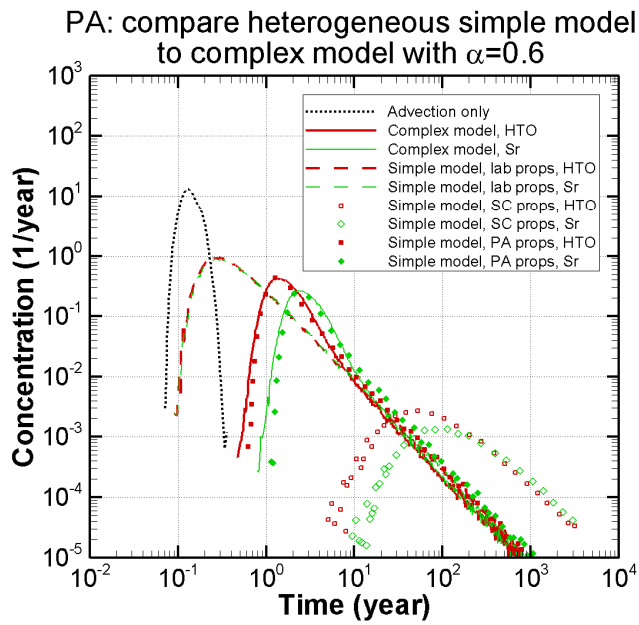
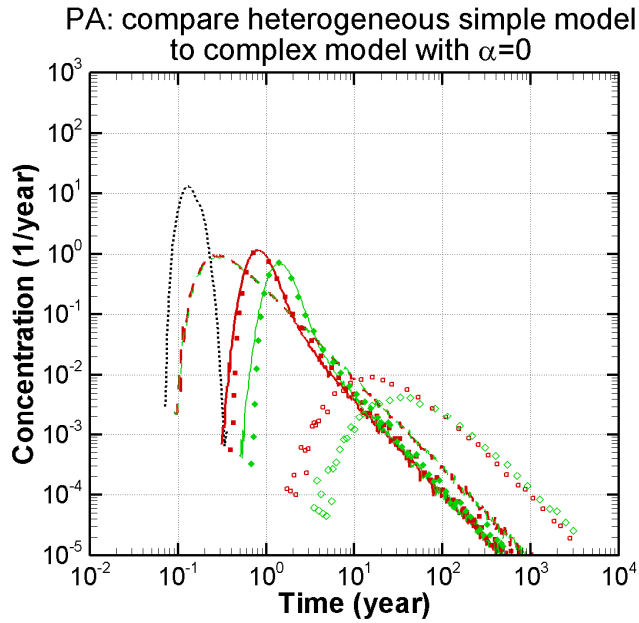
792

793 Figure 9. SC tracer BTCs for the complex fracture model and two versions of the uniform
 794 simple fracture model (the original model with laboratory-measured properties and the
 795 model calibrated to SC), for two values of fracture structure parameter α . Results for
 796 advection-only through a uniform fracture with $\alpha = 0$ are also shown.



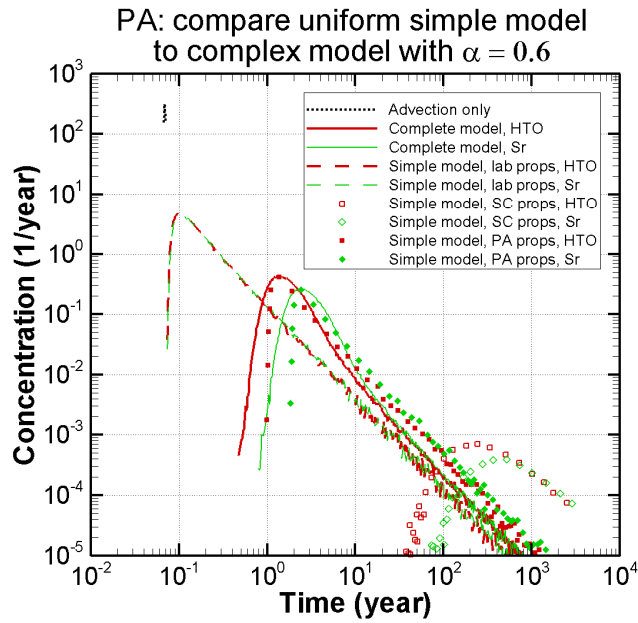
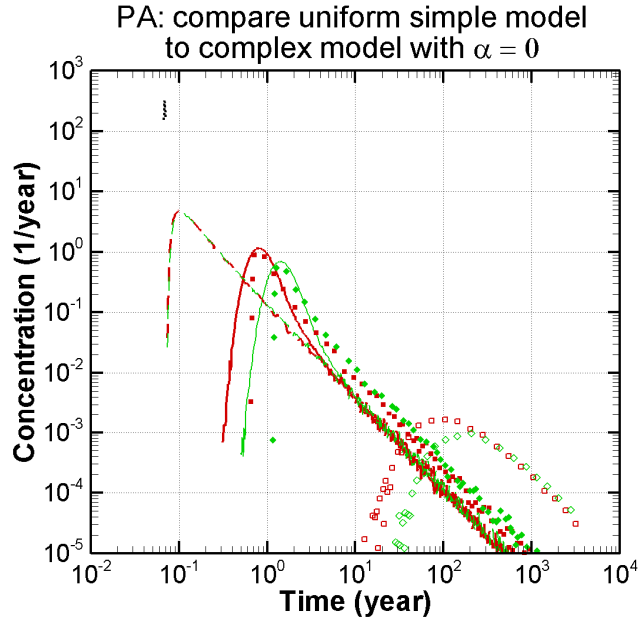
797

798 Figure 10. Simplified model parameters required to match SC tracer BTCs for the
 799 heterogeneous simple model (het) and the uniform simple model (uni), for a range of α
 800 values. The vertical axes show the ratio of the calibrated parameter to the original
 801 laboratory-measured values (two left columns) or the ratio of the calibrated parameters
 802 for SC and PA (right column).



803

804 Figure 11. PA tracer arrivals for the complex fracture model and three versions of the
 805 heterogeneous simple fracture model (the original model with laboratory-measured
 806 properties, the model calibrated to SC, and the model calibrated to PA), for two values of
 807 fracture structure parameter α . Results for advection-only through a heterogeneous
 808 fracture with $\alpha = 0$ are also shown.



809

810 Figure 12. PA tracer arrivals for the complex fracture model and three versions of the
 811 uniform simple fracture model (the original model with laboratory-measured properties,
 812 the model calibrated to SC, and the model calibrated to PA), for two values of fracture
 813 structure parameter α . Results for advection-only through a uniform fracture with $\alpha = 0$
 814 are also shown.